

On the InGaAs-based Photodetection Circuit for Scanning Near-Infrared Signal in the Wavelength Range of 1.0-2.0 μm

Kuntao Ye^{1,*} and Xin Li¹

Abstract: Detection of scanning long wave near-infrared (NIR) signal is critical in numerous applications spanning the fields of military, industry, agriculture, environment, and medicine. In this paper, we present a low cost, high performance InGaAs-based photoelectric conversion and amplification circuit for detecting scanning NIR signal in the wavelength range of 1.0-2.0 μm . With a special focus on reducing the influence of dark current and dark current noise for improved detector efficiency and precision, this proposed circuit features a photovoltaic preamplifier, a low-pass filter, and a temperature control unit; the signal gain, the bandwidth and the noise of the entire circuit is tuned for the signal spectrum of interest. In particular, to make the InGaAs detector operate at the target temperature with little fluctuation, a low-cost closed-loop temperature control circuit is designed that delivers temperature control accuracy of $\pm 0.1^\circ\text{C}$. Both simulation and experimental results have confirmed that the proposed detection circuit meets the specific performance requirements for its intended use in spectrometer.

Keywords: InGaAs, TEC, Sallen-Key, Temperature control.

1. Introduction

Due to its high efficiency and low dark current at room temperature^[1], InGaAs photodiode detector along with its concomitant photoelectric conversion and amplification circuit has found its great use in military, industrial, agricultural, environmental, and medical applications for the long wave near-infrared (NIR) wavelength range^[2].

Like any other photodiode detector, dark current of InGaAS-based detector remains one of the most important limiting factors in photoelectric detection efficiency, and dark current noise is often a dominating noise source. Besides diode geometrical configuration^[1], process or doping concentrations^[3], bias voltage and operating temperature are the two most significant factors to the generation of dark current, especially when an InGaAs diode detector gets deployed in the field. Correspondingly, proper selection of bias voltage and accurate control of the operating temperature are critical in InGaAs diode detector along with its accompanying photoelectric conversion and amplification circuit.

Photoelectric conversion and amplification circuit should be designed to ensure that the photodetector is biased to operate at the photovoltaic mode rather than at the photoconductive mode for lower dark current, lower dark current noise, higher linearity for optical power detection^[4, 5]. Besides setting up the appropriate bias and operating points in InGaAS-based detector, temperature control is needed for the purposes of reducing the dark current or other thermal noise and improving the detection efficiency and precision. It was shown in the near-infrared (NIR) in the wavelength

¹ Institute of Medical Information Engineering, School of Science, Jiangxi University of Science and Technology, Hongqi Ave. No. 86, Ganzhou, 341000, China.

*Corresponding Author: Kuntao Ye. Email: kuntaoye@126.com.

range of 1.0-2.0 μm that the photo detection precision is highly related to the operating temperature of the detector and temperature fluctuation^[6].

In the literature, a large number of InGaAs detectors working at the photovoltaic mode^[7, 8] have been reported. These designs tend to be quite expensive, and they are application-specific, rendering them unsuitable for the application of low cost, long wave NIR spectrometer.

In this paper, we thus present a low cost photoelectric conversion and amplification circuit for the NIR spectrometer in the wavelength range of 1.0 to 2.0 μm . This circuit features a photovoltaic preamplifier, a low-pass filter amplification circuit, and a temperature control circuit. The signal gain, the bandwidth and the noise of the entire circuit is tuned for a spectrometer of interest. In particular, to make the InGaAs detector operate at the target temperature with low temperature fluctuation, a low-cost closed-loop temperature control circuit is designed.

2. Photoelectric conversion and amplification circuits

To achieve low noise, high detection efficiency of the InGaAs detector, a thermoelectric cooler (TEC) is built into the InGaAs detector for closed-loop temperature control to assure that the detector continuously operates at a constant low temperature. This temperature control circuit needs to easily set to accommodate different target temperatures. Besides the noise issue, for a long wave NIR spectrometer in the wavelength of 1.0 to 2.0 μm , with a spectral resolution of 10nm and a resonance frequency of 50 Hz, the frequency bandwidth of the photoelectric conversion and amplifier circuit has to be able to operate in the frequency band of 80-200 KHz^[9].

The circuit architecture of the photoelectric conversion is shown in figure 1. When the optical signal hits the InGaAs detector working at the photovoltaic mode, the detector (G5853-11 InGaAs detector) converts the electrical current, resulting from the photoelectric effect, into voltage, and then the voltage signal gets amplified by the preamplifier that is essentially a resistively loaded transimpedance amplifier (RTIA)^[10]. The amplified signal coming out of the RTIA needs to be further filtered and amplified by passing through a low-pass filter as shown in figure 1.

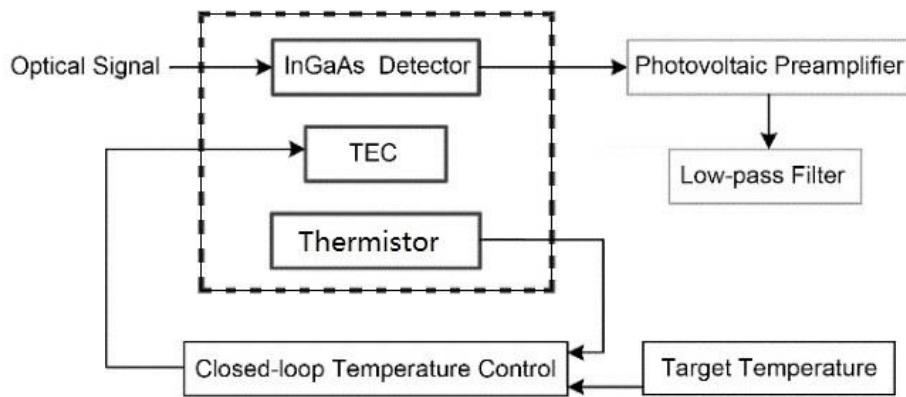


Figure 1: Photoelectric conversion system block diagram.

2.1. Preamplifier and filter circuit

The equivalent circuit of the G5853-11 InGaAs detector, shown in figure 2, consists of (1) the shunt capacitor, C_d , which is the junction capacitor of the diode, (2) the series resistor, R_s , and (3) the shunt resistor R_d . The values of C_d , R_s , and R_d that are marked in figure 2 are from the manufacture.

In figure 2, it also shows the stray capacitor of the feedback resistor R_f , denoted as C_s , which is normally smaller than 1pF.

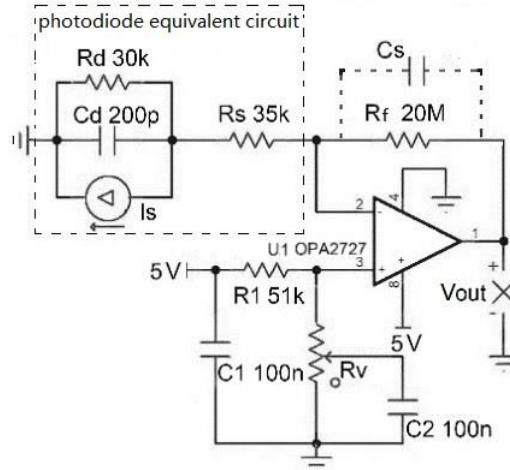


Figure 2: The preamplifier circuit

The signal gain A_s and the noise gain A_N of the preamplifier circuit shown in figure 2 are given below.

$$A_s = U_{out} / I_s = \frac{(R_s + R_f)(1+jf / f_z)}{(1+jf / f_p)(1+jf / f_x)} \tag{1}$$

$$A_N = e_{no} / e_{ni} = \left(1 + \frac{R_f}{R_s + R_d}\right) \frac{1+jf / f_{z1}}{(1+jf / f_{p1})(1+jf / f_x)} \tag{2}$$

where f_x is the frequency where the signal gain and the noise gain are equal to the open loop gain of the op-amp^[11], and

$$f_z = \frac{1}{2\pi(R_f \parallel R_s)C_d} \tag{3}$$

$$f_p = \frac{1}{2\pi R_f(C_d + C_s)} \tag{4}$$

$$f_{z1} = \frac{1}{2\pi(R_d \parallel (R_f + R_s))C_d} \tag{5}$$

$$f_{p1} = \frac{1}{2\pi(R_d \parallel R_s)C_d} \tag{6}$$

From equations (1) through (6), one can see that both the signal gain A_s and the noise gain A_N increase with the increase of the feedback resistance of R_f ; on the other hand, smaller resistance value of R_f corresponds to a wider bandwidth, but a smaller signal gain. Since the bandwidth and the signal gain of the circuit go the opposite direction, trade-offs have to be made when selecting the value of R_f . For an amplifier that requires a wider frequency band, a single stage of amplification may not be able to provide the signal gain needed, and a second stage of amplification has to be added before A/D conversion, as the case in this study.

Low noise CMOS FET OPA2727 is selected at the input stage of RTIA to achieve low noise performance. The OPA2727 has the gain bandwidth product (GBP) of 20 MHz, noise of $6nV/\sqrt{Hz}$ Hz at 100 KHz. By swinging the precision resistance R_v , from 0 to 1 K Ω , the dc level of the output voltage signal changes accordingly.

The cut-off frequency of the photoelectric conversion amplifier circuit in figure 2 can be expressed as

$$f_h = \sqrt{GBP / (2\pi R_f C_{in})} \tag{7}$$

where GBP is the gain bandwidth product of the op-amp, and C_{in} is the lumped input capacitance. Since the bandwidth is expected to be 200KHz, for the given GBP of the op-amp, the feedback resistance R_f is estimated to be 20.28M Ω from equation (7).

For practical reasons, a resistor with resistance of 20M Ω is selected for R_f in the actual implementation. Correspondingly, the bandwidth of the RTIA circuit is 201.4 KHz calculated from equation (7), and 210.7 KHz from simulation using TINA-TI 9 software.

Signal output from the preamplifier circuit with appropriate bandwidth and smaller signal gain needs to be further amplified to match the input requirements of the A/D conversion. In order to further reduce the noise and maintain the desired signal bandwidth, a Sallen-Key low-pass filter circuit is designed as shown in figure 3. The values of all the components in the circuit are chosen to deliver a gain of 3.2 (or 9.6 dB) and a bandwidth of 201.8 KHz.

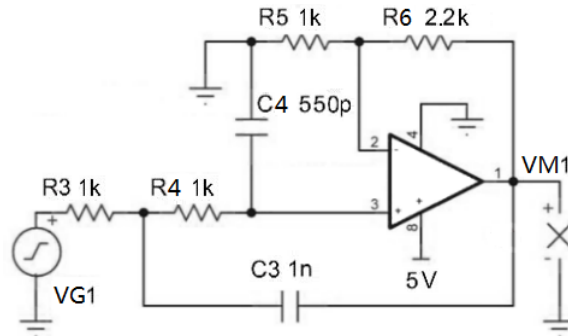


Figure 3: The low-pass filter

2.2. Temperature control circuit

The feedback closed-loop temperature control circuit, shown in figure 4, is made up of the temperature acquisition circuit, the differential amplifier, the analog PID control circuit and the TEC driving circuit. Note that R_{12} is the thermistor, and the diode TL431 provides a 2.5V high-precision reference voltage for both R_8 and R_{12} . The voltage V_f across R_{12} changes with the temperature. The voltage follower U4B's output voltage V_f drives the A/D converter (not shown in figure 4), which tracks the temperature variation.

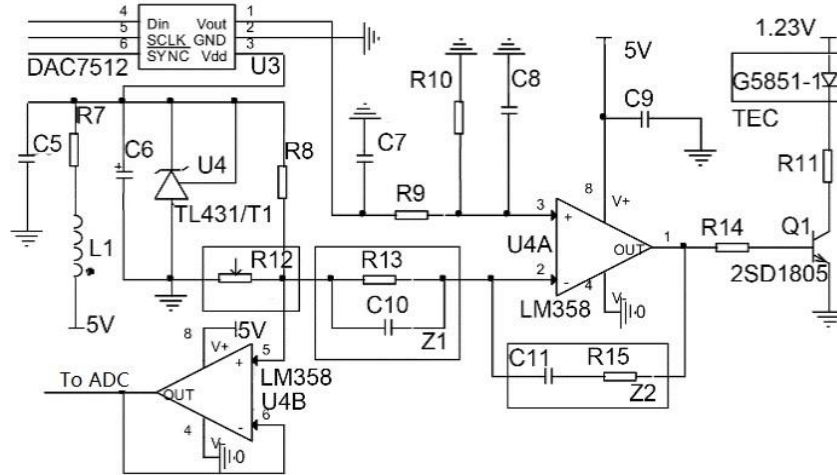


Figure 4: The temperature control circuit.

DAC7512, a D/A converter, is used for setting the voltage at the op-amp input node 3, which corresponds to different target temperatures. The input and feedback of the PID control circuit consists of the components of U4A, R_{13} , R_{15} , C_{10} , C_{11} .

To avoid the maximum cooling current exceeding the limitation of TEC unit, R_{14} is set to be $1k\Omega$, and the bipolar transistor 2SD18050 is chosen to provide the cooling current flowing through the device.

Assume that the thermal inertia for both the built-in TEC unit and the thermistor that is part of the InGaAs detector can be modeled as a first-order process. The transfer function of the temperature control circuit in figure 4 is thus given as ^[12]:

$$G(s) = \frac{k}{T_i s + 1} e^{-\tau s} \tag{8}$$

where T_i is the time constant of the cooler TEC, τ is a pure time constant, and k is the proportional constant. Unfortunately, all these parameters of the TEC unit and thermistor are normally unknown, and they have to be dealt with following a procedure described below

The PID controller, with its output voltage of $u(t)$ is modelled as:

$$u(t) = K_p e + K_i \int e dt + K_d \frac{de}{dt} \tag{9}$$

where K_p is the proportional gain, K_i is the integral gain, K_d is the derivative gain.

In figure 4, it can be seen that

$$Z_1(s) = R_{13} \parallel \frac{1}{sC_{10}} = \frac{R_{13}}{1 + sC_{10}R_{13}} \tag{10}$$

$$Z_2(s) = R_{15} + \frac{1}{sC_{11}} \tag{11}$$

$$U_o(s) = \frac{Z_2(s)}{Z_1(s)} \Delta V_i(s) = \frac{R_{15}}{R_{13}} + \frac{C_{10}}{C_{11}} + sC_{10}R_{15} + \frac{1}{sC_{11}R_{13}} \quad (12)$$

Taking the inverse Laplace transformation of equation (12), one can get the signal representation in time domain,

$$u_o = \left(\frac{R_{15}}{R_{13}} + \frac{C_{10}}{C_{11}}\right)\Delta v_i + C_{10}R_{15} \frac{d\Delta v_i}{dt} + \frac{1}{C_{11}R_{13}} \int \Delta v_i dt \quad (13)$$

Inspection of equations (9) and (13) reveals that:

$$\begin{cases} \frac{R_{15}}{R_{13}} + \frac{C_{10}}{C_{11}} = K_p \\ C_{10}R_{15} = K_i \\ \frac{1}{C_{11}R_{13}} = K_d \end{cases} \quad (14)$$

Based on equation (14), the temperature control circuit shown in figure 4 can be abstracted to build a control model shown in figure 5, where the main loop contains four cascaded stages: from left to right, (1) the gain stage with a gain of K_1 , (2) a PID controller with a transfer function of $PID(s)$, (3) transconductance (ratio of collector current to transistor base voltage) with a transfer function of β/R , (4) a first-order inertia TEC system with a delay time constant τ . The feedback loop realizes function of $U_i(T)$, the static voltage of the thermistor with respect to temperature that is detected by the thermistor within the TEC.

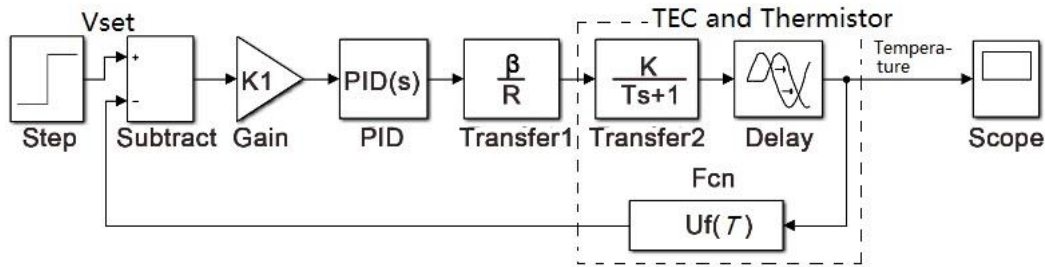


Figure 5: The model for the temperature control.

The PID is iteratively optimized to find the values of K_p , K_i , and K_d , after which the values of the actual circuit components (R_{15} , R_{13} , C_{10} , C_{11}) can be determined through equation (14).

When C_{10} , C_{11} are absent from the circuit, then according to equation (14), $K_p = R_{15}/R_{13}$, and $K_i = K_d = 0$, the circuit is actually a differential amplifier with a feedback for closed-loop temperature control. In this case, the system is nothing but a simple proportional control that can be described as

$$u_o = -\frac{R_{15}}{R_{13}} U_f + \left(1 + \frac{R_{15}}{R_{13}}\right) \left(\frac{R_{10}}{R_{10} + R_9}\right) v_i \quad (15)$$

3. Results

To verify the design of the proposed photoelectric conversion circuit along with the closed-

loop temperature control, a PCB circuit board is produced. The HL-2000 halogen light source is used as the input to a long wave NIR spectrometer based on MEMS micromirror at room temperature of 26°C. The incident light source is reflected back to the InGaAs detector by the MEMS micromirror with a scanning frequency of 50 Hz. The light pulse has a square waveform with peak-to-peak voltage of 10 V and duty ratio of 25%, which means the MEMS micromirror completes two spectral scans within 20 ms in one round trip.

The detected scanning NIR spectral signal is amplified by the photoelectric conversion amplifying circuits. A Tektroix oscilloscope reads the output waveform from the photoelectric conversion amplifying circuit, and the data of one scanning period at temperatures of 1°C, -5°C and -10°C are all shown in figure 6.

The output signal with a peak of 1.79 V at room temperature satisfies the requirements put forth by the subsequent data acquisition. And one can see that the noise level of the output at room temperature is the. The smoothest output wave at -10°C indicates the lowest noise level, which has a peak of 2.11 V. This experiment result shows when temperature control circuit is employed, the dark current and the influence of dark current noise on the signal are significantly suppressed.

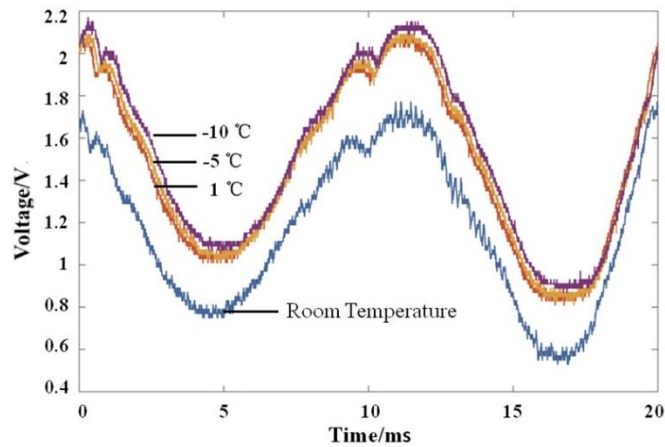


Figure 6: Output signal from the InGaAs-based photodetection circuit at different temperature. Temperature variations in the cooling process are also measured, and the result is shown in figure 7. It can be noticed that at the beginning, the temperature decreases quickly, and reaches a stable level after about 20s. When the temperature of the InGaAs detector measured through the thermistor is stabilized, temperature fluctuation is confined to be within $\pm 0.1^\circ\text{C}$. This experiment confirms that the entire process indeed follows a typical first-order inertia process as assumed in Section 2.

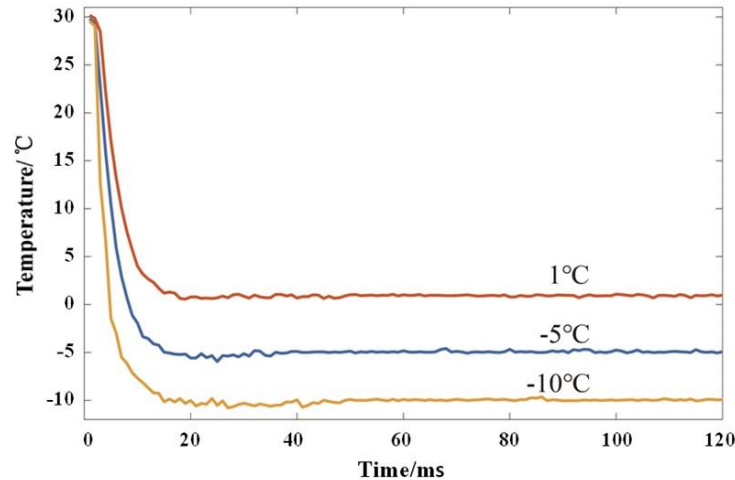


Figure 7: Variation of temperature for different target temperatures in the temperature control process

4. Conclusions

This paper presented detailed design of a low cost, low noise photoelectric conversion amplifying circuit for InGaAs detector with build-in TEC unit and thermistor. The temperature control circuit in particular helps the InGaAs detector to operate at stable temperature level with temperature fluctuation is well controlled to be within $\pm 0.1^\circ\text{C}$. As a result, both the dark current level and the dark current noise, the two major factors impacting detector efficiency, are considerably suppressed, leading to much improved detector efficiency.

References:

1. **M. Verdun,; G. Beaudoin,; B. Portier,; N. Baardou,; et al.**, "Dark current investigation in thin p-i-n InGaAs photodiodes for nano-resonators," *Journal of Applied Physics*. **120**(084501), 1-6 (2016).
2. **A. Rogalski**, "Infrared detectors status and trends," *Progress in Quantum Electronics*. **27**, 59-210 (2003).
3. **Y. Zhao,; D. Zhang,; L. Qin,; Q. Tang,; et al.**, "InGaAs-InP avalanche photodiodes with dark current limited by generation-recombination," *Optics Express*. **19**(9), 8546-8552 (2011).
4. **L. Dan,; R. Massom**, *Polar Remote Sensing 1 Atmosphere and Oceans* (Book), Springer Published in association with Praxis Publishing, Chichester UK (2006).
5. **J. Wen,; W. J. Wang,; X. R. Chen,; N. Li,; et al.**, "Origin of large dark current increase in InGaAs/InP avalanche photodiode," *Journal of Applied Physics*. **123**(161530), 1-5 (2018).
6. **Prochazka**, "Peltier-cooled and actively quenched operation of InGaAs/InP avalanche photodiodes as photon counters at a 1.55-um wavelength," *Applied Optics*. **40**(33), 6012-6018 (2001).
7. **Lasobras,; R. Alonso,; C. Carretero**, "Infrared sensor-based temperature control for domestic induction cooktops," *Sensors*. **14**, 5278-5295 (2014).
8. **M. Akiba,; Y. Kanai**, "Ultrahigh-sensitivity infrared detection system using an InGaAs p-i-n photodiode with low dielectric polarization noise," *Optics Letters*. **37**(12), 2235-2237 (2012).
9. **Ye,; T. Dong,; W. He,; Y. Li,; et al.**, "Design and implementation of a long wavelength near infrared spectrometer based on MEMS scanning mirror," *Spectroscopy and Spectral Analysis*.

- 34**(10), 2858-2862 (2014).
10. **B. Mishra; K. Sharma; P. Choudhary**, "A low noise Op-Amp transimpedance amplifier for InGaAs photodetectors," *International Research Journal of Engineering and Technology*. **2**(5), pp 54-58 (2015).
 11. **Yang; L. Hu; Y. Duan; S. Mao**, "The design of the amplifier for weak photoelectric current signal," *Nuclear Electronics & Detection Technology*. **31**(9), 734-738 (2011).
 12. **H. Cao; Y. Yang; S. Liu; W. Zhao**, "Temperature control system for SLD optical source of FOCS," *Infrared & Laser Engineering*. **43**(3), 920-926 (2014).